SCIENTIFIC REPORTS

OPEN

SUBJECT AREAS:
EARTH SCIENCES
CLIMATE CHANGE
ATMOSPHERIC SCIENCE
PALAEOCLIMATE

Received
3 July 2012

Accepted
15 August 2012

Published
31 August 2012

Correspondence and requests for materials should be addressed to Z.A. (anzs@loess.llqg.ac.cn)

Interplay between the Westerlies and Asian monsoon recorded in Lake Qinghai sediments since 32 ka

Zhisheng An[1,2], Steven M. Colman[3], Weijian Zhou[1], Xiaoqiang Li[1], Eric T. Brown[3], A. J. Timothy Jull[4], Yanjun Cai[1], Yongsong Huang[5], Xuefeng Lu[1], Hong Chang[1], Yougui Song[1], Youbin Sun[1], Hai Xu[1], Weiguo Liu[1], Zhangdong Jin[1], Xiaodong Liu[1], Peng Cheng[1], Yu Liu[1], Li Ai[1], Xiangzhong Li[1], Xiuju Liu[3], Libin Yan[1], Zhengguo Shi[1], Xulong Wang[1], Feng Wu[1], Xiaoke Qiang[1], Jibao Dong[1], Fengyan Lu[1] & Xinwen Xu[1]

[1]State Key Laboratory of Loess and Quaternary Geology, Institute of Earth Environment, Chinese Academy of Sciences, Xi'an, 710075, China, [2]Department of Environmental Science & Engineering, Fudan University, Shanghai 200433, China, [3]Large Lakes Observatory and Department of Geological Sciences, University of Minnesota Duluth, Duluth, MN 55812, USA, [4]NSF Arizona AMS Facility, University of Arizona, Tucson, AZ 85721, USA, [5]Department of Geological Sciences, Brown University, Providence, Rhode Island 02912, USA.

Two atmospheric circulation systems, the mid-latitude Westerlies and the Asian summer monsoon (ASM), play key roles in northern-hemisphere climatic changes. However, the variability of the Westerlies in Asia and their relationship to the ASM remain unclear. Here, we present the longest and highest-resolution drill core from Lake Qinghai on the northeastern Tibetan Plateau (TP), which uniquely records the variability of both the Westerlies and the ASM since 32 ka, reflecting the interplay of these two systems. These records document the anti-phase relationship of the Westerlies and the ASM for both glacial-interglacial and glacial millennial timescales. During the last glaciation, the influence of the Westerlies dominated; prominent dust-rich intervals, correlated with Heinrich events, reflect intensified Westerlies linked to northern high-latitude climate. During the Holocene, the dominant ASM circulation, punctuated by weak events, indicates linkages of the ASM to orbital forcing, North Atlantic abrupt events, and perhaps solar activity changes.

Lake Qinghai (36°32′–37°15′N, 99°36′–100°47′E), the largest lake in China, is a closed-basin, brackish lake, situated in the sensitive semi-arid zone between the ASM-controlled (humid) and the Westerlies-influenced (arid) areas of Asia (Supplementary Fig. S1). The mean annual temperature in this drainage basin is ~ –0.1°C, and the mean annual precipitation is ~373 mm, with more than 65% occurring in summer (Supplementary Fig. S1). At present, the ASM circulation reaches this region in summer (Fig. 1a) while the Westerlies climate dominates in winter (Fig. 1b), resulting in a clear seasonality of precipitation (Supplementary Fig. S1). During the last glacial maximum (LGM), model results indicate that the summer monsoon weakened and the Westerlies, which transmitted climate signals from North Atlantic and Greenland[1], were strengthened significantly (Supplementary Fig. S2). However, compared to eastern China, the East Asian winter monsoon does not directly influence the northeastern TP because of its high elevation. This observation is supported by reconstructed trajectories of cold-air surges in winter[2], by modern climatological observations, and by reanalysis of LGM modeling results (Supplementary Fig. S3, Text S1). Thus, Lake Qinghai is an ideal site to study the competing influence of a two-component system comprised of the Westerlies and the ASM on the northeastern TP in the past, and then to provide a basis for understanding the changes of these two sub-systems under the scenario of global warming in the future.

With the support of the International Continental Drilling Program (ICDP), Lake Qinghai was drilled in 2005 using the ICDP GLAD800 drilling system. The longest and highest quality drilling cores, 1F and 1A (36°48′40.7″N, 100°08′13.5″E, 3194 m above sea level) were obtained from the deposition-center of the south-western sub-basin of Lake Qinghai[3]. We used lithological and proxy data from cores 1F and 1A to create a composite record (1Fs, Supplementary Fig. S4). Sediments were sampled at 1 cm intervals and measured for grain size, $CaCO_3$, and total organic carbon (TOC) for the whole composite core. Ostracod $\delta^{18}O$ values were measured

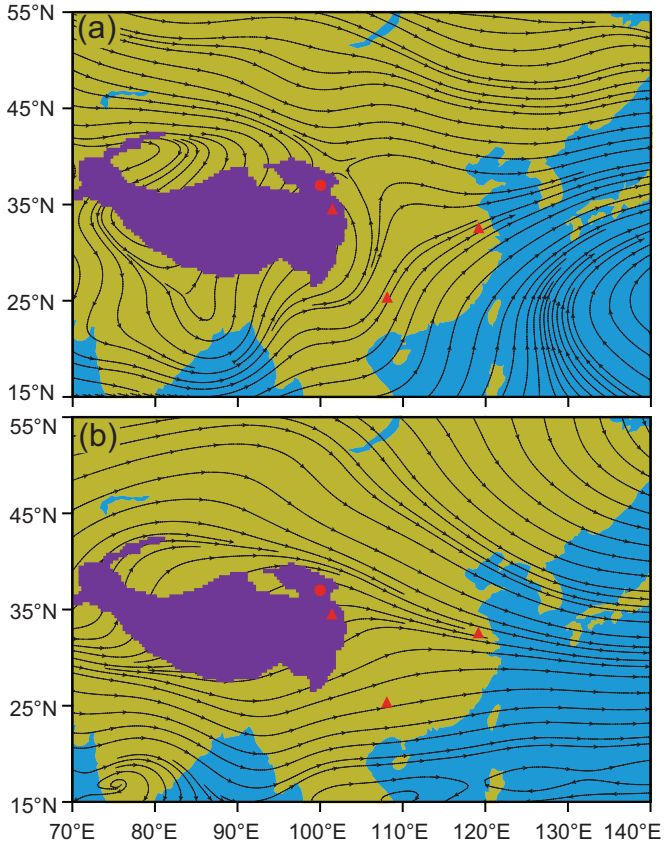

Figure 1 | Averaged atmospheric flow fields at 700 hPa isobaric: (a) in summer (JJA) and (b) in winter (DJF) from 1971 to 2000[54]. Red solid circle, Lake Qinghai (36°32′–37°15′N, 99°36′–100°47′E, elevation 3194 m); triangles indicate the caves mentioned in the text, Xiannv cave (34°27′N, 101°26′E, elevation 3730 m, ~250 km southeast of Lake Qinghai); Dongge cave (25°17′N, 108°5′E); Hulu cave (32°30′N, 119°10′E). The purple shaded area indicates the region where the elevations exceed 3000 meters (i.e. the Tibetan Plateau).

for the upper 5.0 m of the core. These physical, geochemical, and stable isotopic proxies were then used to study the climate changes at Lake Qinghai associated with the interplay of the Westerlies and the ASM.

Results

The upper 5.0 m of 1Fs is composed mainly of dark gray to light brown lacustrine silty clay or clay with horizontal bedding. The middle part (5.0–9.0 m) is composed of gray and grayish-yellow silty clay with silt layers, suggesting a mixture of shallow lake and loess-like sediments. Light brown and gray silty clay, with loess-like silt and fine sand layers are present in the lower part (9.0–18.6 m) of the core (Supplementary Fig. S4).

Sixty-five samples from cores 1F and 1A were measured for ^{14}C dating, including 52 bulk (TOC), 6 *Ruppiaceae* seed, and 7 plant residue samples (Supplementary Table S1). Ages were determined at both the Xi'an and Tucson AMS facilities, and the results from the two laboratories agree well (see Materials and methods, Supplementary Table S2). With the exception of 8 anomalous ages, the remaining 57 ages were calibrated and used to establish the age model for the 1Fs (see Materials and methods).

Based on the lithologic differences in 1Fs, separate linear regressions were applied to the calibrated ages of three sections, 0–5.0 m, 5.0–9.0 m and 9.0–18.6 m, respectively (Supplementary Fig. S5). Using these regressions, the average reservoir effects for these sections are calculated to be 135, 1143, and 2523 yrs (see Materials and methods). We interpret these results to imply an increasing proportion of organic matter containing old carbon of terrestrial origin[4,5], and perhaps increasing groundwater influence, with increasing depth. These regressions represent long-term average estimates of the reservoir effect; fluctuations in the reservoir effect may exist on shorter time scales. Comparison of our summer monsoon proxy with the speleothem $\delta^{18}O$ record in a neighboring region further supports our chronology (Supplementary Fig. S6). Compared with previous studies[6,7], we obtained many more ^{14}C analyses and better constrained likely reservoir effects, so that the present chronology may be the optimum for Lake Qinghai sediments, and our proxy climatic records are chronologically more comparable with global climatic records.

Lake Qinghai sediments mainly consist of detrital materials of riverine and eolian origins, combined with authigenic carbonates[8]. Grain-size distribution patterns vary significantly in different lithological units. Detailed comparisons among the grain-size distributions of modern dust, loess, surface lacustrine sediments, and suspended particles from the largest river in the catchment suggest that 25 μm is a good threshold value for differentiating riverine components and dust-fall contributions in Lake Qinghai (Supplementary Fig. S7, see Materials and methods). Grain-size distributions in core 1Fs are also characterized by two populations with a boundary at about 25 μm (Supplementary Fig. S7); fine and coarse populations mainly correspond to the riverine and eolian input, respectively. Therefore, content of >25 μm fraction of lake sediment is considered as an indicator of the eolian contribution to the sediments. Variations in the content of >25 μm fraction indicate that riverine components dominated in the Holocene, and that eolian components dominated during the 11.5–32 ka interval (Fig. 2). Before the Holocene, some fine-grained layers with significant decreases in the content of >25 μm fraction exist, suggesting short intervals of riverine dominance, which might be associated with hydrological processes under brief warm-humid conditions.

Previous modeling results indicate that the Lake Qinghai region was close to the surface storm tracks of the Westerlies during the LGM[9]. Lidar observations also reveal a modern "airborne dust corridor" for eastward transport of dust that covers the northern slope and eastern part of the TP[10]. Therefore, in a manner similar to that for the loess deposits linked to the Westerlies in the Ili basin[11,12] and on the northern slope (elevation ~3000 m) of the Kunlun Mountains[13] in Xinjiang, the loess around Lake Qinghai can be regarded as indicative of cold and dry conditions[14] in a climate dominated by the Westerlies. Similar to the way that increased input of coarse fraction in Ili and Kunlun loess indicates intensified Westerlies[11–13], increased >25 μm fraction of Lake Qinghai sediments reflects intensified Westerlies and resultant cold-dry conditions in this region. Here we used the flux of the >25 μm fraction as a Westerlies climate index (WI). Large WI values indicate strengthened Westerlies influence and intensified aridification[15].

Lake Qinghai presently is alkaline and supersaturated with respect to carbonates. Because the total inorganic carbon concentration of modern lake water is high (~4.9 mM) relative to major river and groundwater sources (0.59 to 0.88 mM), and the lake water has much lower Ca^{2+} concentrations (~0.28 mM) than those of rivers or groundwater (~1.4 to 2.2 mM)[16], it is evident that the carbonate chemistry of the lake is Ca^{2+}-limited, and carbonate precipitation (low-Mg calcite and aragonite[16]) balances the amount of Ca^{2+} brought to the lake by river runoff, which in turn relates to regional rainfall. The covariation of carbonate in recent sediments with the observed water discharge of the largest river over the last 50 years[17] further supports this assumption. Because Lake Qinghai apparently was a closed basin for the entire length of our record, the flux of authigenic carbonate to the sediments likely was controlled by the amount of Ca^{2+} brought to the lake by river runoff. Therefore, we propose that carbonate content in Lake Qinghai sediments can be

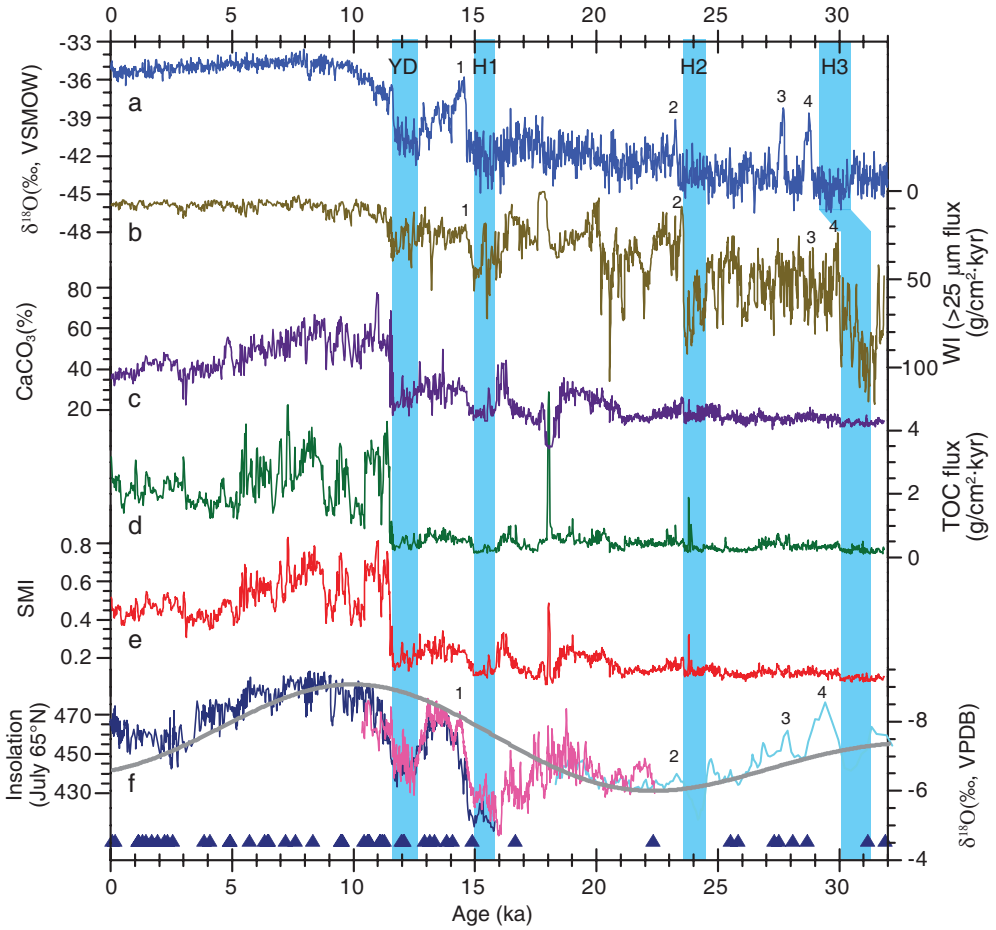

Figure 2 | Comparison of Lake Qinghai records with other records during the last 32 ka. (a) NGRIP $\delta^{18}O$[26]; (b) Lake Qinghai Westerlies climate index (WI, flux of >25 μm fraction); (c) $CaCO_3$ content; (d) total organic carbon (TOC) flux; (e) Lake Qinghai Asian summer monsoon index (SMI); (f) Dongge and Hulu cave speleothem $\delta^{18}O$ records[21,22]. The triangles indicate the ^{14}C dates used for the age model for core 1Fs (Supplementary Fig. S5). The transparent gray curve is July 65°N insolation[55]. The shaded blue bars indicate the cold-dry periods including YD, H1, H2, and H3 events. Numbers indicate glacial interstadials and correlated events at Hulu cave and Lake Qinghai.

used as a proxy for the strength of river runoff and, in turn, the amount of rainfall over the basin, such that high $CaCO_3$ content is related to warm and humid climates associated with strong ASM[7,18].

TOC can also be taken as an indicator of monsoonal precipitation in Lake Qinghai[19]. During strong ASM periods, simultaneous increases in temperature and precipitation cause biomass in the catchment to increase, so that terrestrial organic matter input is enhanced by increased runoff. Meanwhile, relatively warm-wet climatic conditions enhance nutrient supplies and thus increase lake productivity. Enhancement of both terrestrial and aquatic productivity leads to increased TOC in the lake sediments. Because TOC flux is a better measure of the delivery and preservation of organic matter than TOC percentage[20], we calculated the TOC flux and used it as an ASM proxy.

$CaCO_3$ and TOC flux reflect variations in the summer monsoon from the perspectives of carbonate geochemistry and biomass accumulation, respectively. Considering the good correlation between $CaCO_3$ and TOC flux (R^2=0.71) in the sediment sequence, we normalized and averaged these two proxies, creating a non-dimensional Summer Monsoon Index (SMI). Large SMI values represent enhanced summer monsoon climate.

Discussion

The Lake Qinghai SMI record generally resembles the changing trends of ASM records derived from speleothems[21,22] in China over the last 20 ka (Fig. 2). However, the SMI is relatively low and has lower-amplitude fluctuations during the 32 to 11.5 ka interval compared to the speleothem records. Furthermore, the SMI record has an extremely abrupt transition into the Holocene, whereas the cave $\delta^{18}O$ transition is more gradual.

From 32 to 20 ka, our SMI record suggests that the ASM was very weak, exhibiting no long-term change in the mean. We infer that the monsoon front rarely penetrated sufficiently northwest to reach Lake Qinghai, at the fringes of the area affected by the modern ASM. Part of the reason may be that the distance from Lake Qinghai to the oceanic moisture source increased during the LGM, when the coastline moved southeastward by as much as 1000 km (Supplementary Fig. S8). This implies that long distance translation of the coastline in East and Southeast Asia associated with the sea-level change may have played an important role in regulating the summer monsoon over inland Asia on glacial-interglacial timescales. After 20 ka, the SMI indicates slight strengthening of the ASM and then an abrupt increase at 11.5 ka, consistent with the abrupt rises in sea level and associated tropical ocean warming[23], and the timing of rapid rise of sea level resulting from the Melt Water Pulse 1B[24], respectively. These factors likely contributed to the strengthening of the ASM through increased moisture supply at these times. During the Holocene, both the amplitude and variability of the ASM increased markedly, especially in the early Holocene, suggesting the front of intensified summer monsoon penetrated to Lake Qinghai and even further inland. This is consistent with a relatively high lake level in the early Holocene[6]. The weakened ASM during the last glaciation and the

strengthened ASM in the Holocene broadly support insolation as a major control on the ASM[25] (Fig. 2).

The WI indicates that the mid-latitude Westerlies climate dominated the Lake Qinghai area in glacial times and that the strength and variability of the Westerlies climate were notably larger than during the Holocene. Our data and previous studies[6] suggest that the basin was occupied by a shallow, brackish water body under cold, arid and windy conditions. This pattern of WI variation is generally similar to that of NGRIP $\delta^{18}O$ record[26] during the last 32 ka, although the WI exhibits higher amplitude fluctuations in the pre-Holocene interval (Fig. 2). Global climate modeling has demonstrated that ice sheet growth and lower North Atlantic sea-surface temperature during the LGM led to an increase in the meridional (latitudinal) temperature gradient and southward migration of the polar front and the Westerlies[9,25]. Therefore, the Westerlies are most likely the link between the climatic variations in the high north latitudes and the northeastern TP.

Over the past 32 kyr, the Westerlies systematically weakened while the ASM climate strengthened beginning at 20 ka, especially after 11.5 ka. Thus, there is an anti-phase relationship between the Westerlies and the ASM climates on glacial-interglacial timescales (Fig. 2). This kind of interplay can be ascribed to forcing by north hemisphere insolation, ice volume, and associated high north-latitude climate and sea level changes.

Abrupt, large-amplitude increases in the WI, most of which correlate well with changes in the NGRIP $\delta^{18}O$ record, a phenomena similar to the loess deposits in the Ili Basin[12], indicate markedly intensified Westerlies climate during the Younger Dryas (YD), LGM, and (within the relative accuracies of the lake and ice core chronologies) Heinrich events 1, 2 and 3 (Fig. 2). These cold-dry and dust-rich events are marked by visible loess-like sediments and by increases in the coarse fraction, suggesting strong instabilities in the Westerlies-dominated climate during glacial times. Strengthening (or weakening) of the Westerlies on the TP could be produced by shifts in the mean position of the Westerlies. During these cold events, the core of the Westerlies shifted southward to a position over Lake Qinghai during times when the North Atlantic Ocean was cold and relatively ice-covered. This would be consistent with studies that have documented southward shifts of other climate systems such as the Intertropical Convergence Zone[27] or the Southern Hemisphere Westerlies[28]. Contemporaneously, muted summer monsoon variation at Lake Qinghai and weakened ASM indicated by the speleothem $\delta^{18}O$ records demonstrate an anti-phase relationship between the ASM and Westerlies-dominated climates on millennial timescales. Within these events, increased frequency of dust storms, represented by high WI values, suggests large variability in the Westerlies climate on centennial timescales. Even with the uncertainty of our chronology, the WI suggests damped Westerlies influences during DO oscillations 1 to 4 (Fig. 2). It is plausible that cold air excursions of high-latitude, North Atlantic origin influenced the climate on the northeastern TP, and also caused cold-dry events in the East Asian monsoon areas, having been transmitted through the Westerlies and the Siberia High[1].

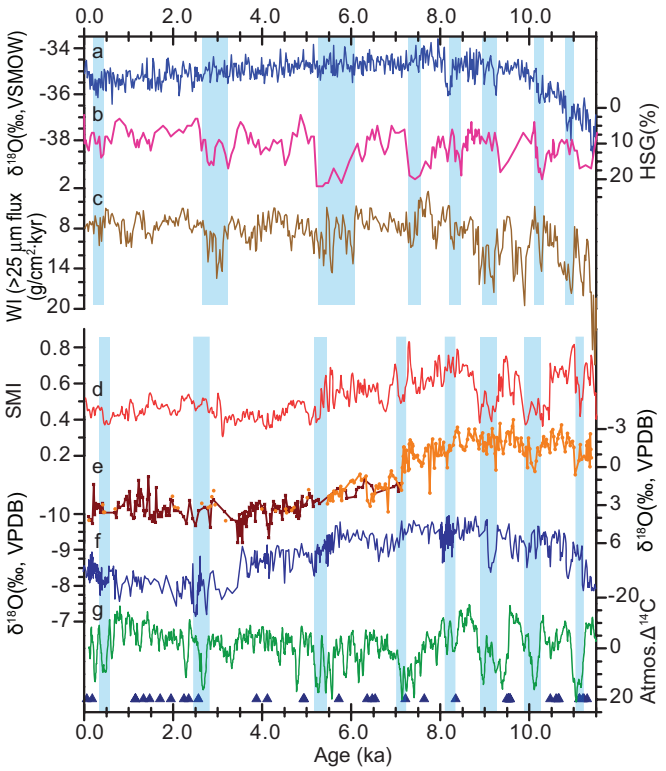

Figure 3 | Comparison of Lake Qinghai records with other records since 11.5 ka. (a) NGRIP $\delta^{18}O$[26]; (b) North Atlantic ice-rafted hematite stained grains (HSG)[29]; (c) Lake Qinghai Westerlies climate index (WI, flux of >25 μm fraction); (d) Lake Qinghai Asian summer monsoon index (SMI); (e) $\delta^{18}O$ record of ostracods from Lake Qinghai: dark brown, *Limnocythere inopinata*; orange, *Eucypris mareotica*; (f) Dongge cave speleothem $\delta^{18}O$[21]; (g) atmosphere $\Delta^{14}C$[38]. The shaded blue bars indicate correlations of various proxies for climatic events. The triangles indicate the ^{14}C dates used for the age model for core 1Fs (Supplementary Fig. S5).

The WI sequence in the Holocene also correlates with the NGRIP $\delta^{18}O$ record[26] in terms of long-term trends, but the WI record differs in having greater amplitude of abrupt climate change at the centennial and millennial scales (Fig. 3). Most of the dry-cold events inferred from increased WI appear to correspond to the Bond events in the North Atlantic[29]. These suggest that the Westerlies may be a cold-air conveyer between the North Atlantic and the northeastern TP in the Holocene as well as in the glacial. In addition, the WI shows oscillations of Westerlies climate from 11.6 to 8.0 ka not recognized in previous work in western China[30].

In the Holocene, the ostracod $\delta^{18}O$ record from Lake Qinghai reflects the precipitation/evaporation budget associated with the ASM system[6,31,32]. In the early Holocene, the depleted $\delta^{18}O$ of *E. mareotica* indicates increases in effective precipitation, implying strengthened monsoon intensity. In contrast, the notably enriched $\delta^{18}O$ values of *L. inopinata*, which are consistent with those of *E. mareotica*[6,31,33], reflect decreased monsoon intensity in the late Holocene. Our high-resolution ostracod $\delta^{18}O$ data show detailed ASM variations with a similar overall trend to that of previous studies (Supplementary Fig. S9, see Materials and methods). Both the SMI and the ostracod $\delta^{18}O$ appear to follow northern hemisphere summer insolation, and document significant ASM variability at millennial time scales in the Holocene, as does the $\delta^{18}O$ record from Dongge Cave (Fig. 3). This SMI variability may be linked to North Atlantic abrupt events associated with the Atlantic's overturning circulation and sea-ice variations[34]. The resemblance of two events at 8.2 and 9.3 ka BP implies a common cause and suggests that freshwater forcing played a prominent role in millennial scale climate change[35–37]. Furthermore, weak monsoon events in the SMI sequence can be correlated with many of the intervals of low solar activity (high $\Delta^{14}C$ and low Total Solar Irradiance)[38,39], especially the events around 5.3 and 10 ka. These correlations further support the idea that decreased solar activity may weaken ASM circulation[21,40] through amplifying processes[41].

Spectral analysis of the atmosphere $\Delta^{14}C$ record[42] indicates concentrations of variance at 207 (de Vries), 149, 130, 104, and 88 yrs (Gleissberg) periods. Analysis of the SMI and WI records from Lake Qinghai indicate similar concentrations of variance with a particularly well-resolved peak centered on the Gleissberg period (Supplementary Fig. S10). These findings support the robustness of our Holocene age model and the idea that solar changes are at least partly

responsible for variations in ASM[21,43] and Westerlies climate in the Holocene.

Climatic changes over the semi-arid areas of the TP, as represented by the Lake Qinghai records, are controlled by variations in both the ASM and the mid-latitude Westerlies. In turn, these two circulation systems respond to external forcing (orbital, perhaps solar output) and internal boundary conditions (ice volume, sea-level, and ocean circulation). The Lake Qinghai record exhibits a high degree of sensitivity to changes in these climatic controls. At Lake Qinghai, warm-humid ASM climates are anti-correlated with cold-dry Westerlies climates on glacial-interglacial and glacial millennial scales, and this variation is a manifestation of the interplay between the Westerlies and ASM. The importance of both the ASM and the Westerlies is similar to the case for Lake Hovsgol in the Lake Baikal catchment, where the ASM contributed much moisture during the early Holocene and the Westerlies were dominant during glacial Heinrich events[5]. Similarly, interplay between high- and low-latitude climate variability occurred in the Aegean Sea during the early and middle Holocene[44]. Thus, the alternating influence of the Westerlies and the ASM on glacial-interglacial timescales likely has been a major pattern of climate change in these regions for most of the Quaternary. Enhanced ASM at the boundary between the humid monsoon areas and arid inland regions is most likely associated with increased temperature in Northern Hemisphere. The climatic characteristics reported here provide key observational constraints for understanding climate changes in the humid/arid transition zone in Asia and improving models and their prediction of ASM and Westerlies changes linked to global warming.

Methods

^{14}C dating, data analysis and old carbon correction for core 1Fs. A total of 65 samples (Supplementary Table S1) were processed for ^{14}C dating, among which there are 52 samples of total organic matter (TOC) from bulk sediments, 6 *Ruppiaceae* seeds (from 4.16 to 4.97 m), and 7 plant remains (from 6.70 to 8.38 m). All samples were processed by using 5% HCl to remove all carbonate content before graphitization[45,46]. The graphite preparation for AMS dating is the same as that described by Slota et al.[47] and Jull[48]. Most ^{14}C data were measured at the Xi'an AMS Laboratory. For comparison, 9 replicate ages were obtained from both the Xi'an and Arizona AMS Labs, including graphite leftover from samples measured in Arizona that were re-measured at the Xi'an AMS facility. The replicate results from the two labs agreed well within analytical error (Supplementary Table S2), demonstrating the reliability of the dating results. Additionally, the ^{14}C results for TOC and seeds are in agreement considering their depths in the upper 5 m of core 1Fs (Supplementary Table S3).

Eight ^{14}C samples from 7.36–8.38 m have anomalous ages (17,000–34,000 years older than expected) compared to surrounding samples thought to have reasonable ages (Supplementary Fig. S5). We disregarded these anomalously old ages in creating an age model, and we believe that they may be due to a combination of processes that occurred during deglaciation of the area. Porter et al.[14] found that there are several substantial outwash fans surrounding Lake Qinghai, and that these fans are mainly composed of gravels interstratified with loess and paleosols developed from 33000 to 45000 yr BP (OSL ages)[14]. The structure of ice wedges in the outwash fan suggested that ice melting occurred before loess filled the ice wedge casts ~15000 yr BP (OSL age)[14]. Thus, it is plausible that the meltwater at this time washed out old carbon from these fans and incorporated it in lake deposits during the early period of deglaciation (~16000-18000, based on our age model). Incorporation of this old carbon would result in anomalously old ages. Flushing old carbon into the lake by melting of ice and permafrost may also explain the anomalous values of $CaCO_3$ contents, TOC fluxes, and grain size within this interval. Therefore, we hypothesized that deglacial meltwater processes in the surrounding area might be involved. The remaining 57 dates were used to establish the age model for 1Fs after calibration using CALIB 510[38] and CALPAL2007[49].

According to differences in lithology and TOC content in core 1Fs, we divided the core into 3 sections for age-model purposes: the upper ~4.99 m of lacustrine silty clay to clay; the lower 9.01–18.61 m of silty clay, loess-like silt and fine sand layers; and the transitional unit of silty clay with silt layers from 4.99–9.01 m. We applied linear regressions separately for these three portions (Supplementary Fig S5)[50], as listed below:

$$y_1 = 23.354x_1 + 135,\ R^2 = 0.987,\ \text{equation 1 (0-4.99m)}$$

$$y_2 = 19.973x_2 + 2831,\ R^2 = 0.783,\ \text{equation 2 (4.99-9.01m)}$$

$$y_3 = 12.666x_3 + 10794,\ R^2 = 0.922,\ \text{equation 3 (9.01-18.61m)}$$

Living naked carp (*Gymnocypris przewalskii*), algae, and surface–sediment samples were also dated (Supplementary Table S4), and the ages on surface sediment were included in the age model. The intercept of equation (1) is 135 years, which can be regarded as the average "old carbon" or reservoir age for upper part of the core. The calculated age y_1 (cal yr BP) at depth is the sum of the contributions from the atmospheric ^{14}C at that time and the average old carbon effect. We note that this method does not take into account possible short-term fluctuations in the "old carbon" input, but should be accurate for centennial and longer time scales. Ages for all samples were calculated from these three equations.

Because the top of the second lithological unit (4.99–9.01 m) is not at the surface, the y-intercept for the second equation cannot be used to infer the average old carbon age. However, another way to obtain the average old carbon age for the second interval exists: the difference between the age at 4.99 m calculated from the first regression equation (11654 years) and that calculated from the second regression equation (12797 years). The difference, 1143 years, can be regarded as an average old carbon age for the second portion of the core. Similar calculations yield 2523 years for the average old carbon age of the third (lowest) part of the core. For the second and third portions of the core, the average old carbon ages also rely on the age of the chosen interface point, which could introduce calculation errors.

The increasing average old carbon effect with depth is consistent with the lithology of the core, which changes from the dominance of lacustrine to mix to loess-like facies in the three parts of the core (top to bottom). Increased old carbon effects with depth might be related to an increased supply of terrestrial organic matter containing old carbon[4,5], and perhaps increased groundwater influence, to the lake basin.

Grain size analyses and interpretation. Prior to grain-size measurements, all samples were pretreated by removal of organic matter and carbonates using 15% H_2O_2 and 6M HCl[51], and then dispersed by ultrasonification in a 10 ml 10% $(NaPO_3)_6$ solution. Grain-size distributions were determined using a Malvern 2000 laser instrument. Replicate analyses indicate that the mean grain size has an analytical error of $<2\%$.

In the upper portion of 1Fs (0–11.5 ka), the grain-size distribution of lacustrine sediments is characterized by a unimodal, approximately log-normal, pattern, with mode values ranging from 4 to 12 μm. This grain-size pattern is similar to that of suspended particles in the Buha River, the largest river in the catchment (Supplementary Fig. S7), suggesting that the detritus in the upper part of 1Fs is dominated by riverine input.

The grain-size distributions for the lower part of the core (before 11.5 ka), however, display multiple modes, wide kurtosis and positive skewness, with a dominant mode of 32 to 100 μm. This pattern is similar to size distributions of modern dust and late glacial loess deposits in surrounding areas (Supplementary Fig. S7), suggesting the significant eolian input. These loess samples have been dated by Optically Stimulated Luminescence (OSL), using a Daybreak 2200 reader. The OSL results indicate late glacial ages, ranging from 10.9 ± 0.7 ka to 14.4 ± 1.0 ka, for the loess.

Detailed comparisons among the grain-size results for modern dust, loess, riverine particles, and surface lacustrine sediments suggest that 25 μm is a threshold value for differentiating riverine components from dust-fall contributions (Supplementary Fig. S7). Averaged percentage and standard deviations of each grain-size class of core 1Fs sediments suggest that two grain-size populations exist, with a boundary size of about 25 μm. The fine and coarse populations likely correspond to riverine and eolian inputs to the Lake Qinghai sediments, respectively (Supplementary Fig. S7). Therefore, the content of the >25 μm fraction of lake sediment grain size is considered to be an indicator of the eolian contribution, with higher contents of >25 μm fraction corresponding to more eolian input. Here we used the flux of the >25 μm fraction as an index to the eolian contribution to Lake Qinghai record, which can capture the variations in the eolian component in this changing lithological sequence.

Ostracod analyses. Following the methods described by Li et al.[33,52], ostracod shells were selected and identified for $\delta^{18}O$ measurements. *Limnocythere inopinata* and *Eucypris mareotica* are found in the upper 5.0 m of core 1Fs, where depths 0-3.1 m are dominated by *L. inopinata* and 3.1–5.0 m by *E. mareotica* (Supplementary Fig. S9). The $\delta^{18}O$ values were measured using an isotope-ratio mass spectrometer (MAT-252) with a Kiel II Carbonate Device. The analytical error (2σ) of standards is approximately ±0.2‰ for $\delta^{18}O$[53].

1. Porter, S. C. & An, Z. S. Correlation between climate events in the North Atlantic and China during the last glaciation. *Nature* **375**, 305–308 (1995).
2. Zhang, Y., Sperber, K. & Boyle, S. J. Climatology and interannual variation of the east Asian winter monsoon: results from the 1979–95 NCEP/NCAR reanalysis. *Mon. Weather Rev.* **125**, 2605–2619 (1997).
3. An, Z. S. *et al.* Geophysical survey on the tectonic and sediment distribution of Qinghai Lake basin. *Science in China (Series D. Earth Sciences)* **49**(8), 851–861 (2006).
4. Watanabe, T. *et al.* High-time resolution AMS ^{14}C data sets for Lake Baikal and Lake Hovsgol sediment cores: Changes in radiocarbon age and sedimentation rates during the transition from the last glacial to the Holocene. *Quatern. Int.* **205**, 12–20 (2009).

5. Murakami, T. *et al.* A 27-kyr record of environmental change in central Asia inferred from the sediment record of Lake Hovsgol, northwest Mongolia. *J. Paleolimnol.* **43**, 369–383 (2010).
6. Lister, G. S., Kelts, K. R., Chen, K. Z., Yu, J. Q. & Niessen, F. Lake Qinhai, China: Closed-basin lake levels and the oxygen isotope record for Ostracoda since the latest Pleistocene. *Palaeogeogr. Palaeoclimatol. Palaeoecol.* **84**, 141–162 (1991).
7. Shen, J., Liu, X. Q., Wang, S. M. & Matsumoto, R. Palaeoclimatic changes in the Qinghai Lake area during the last 18,000 years. *Quatern. Int.* **136**, 131–140 (2005).
8. Xu, H. *et al.* Spatial pattern of modern sedimentation rate of Qinghai Lake and a preliminary estimate of the sediment flux. *Chin. Sci. Bull.* **55**, 621–627 (2010).
9. Kutzbach, J., Gutter, P., Behling, P. J. & Selin, R. In *Global Climates since the Last Glacial Maximum*, eds Wright H. E, *et al.* (Univ. of Minnesota Press, MN), pp. 24–93 (1993).
10. Liu, Z. *et al.* Airborne dust distributions over the Tibetan Plateau and surrounding areas derived from the first year of CALIPSO lidar observations. *Atmos. Chem. Phys.* **8**, 5045–5060 (2008).
11. Ye, W. eds, *The Loess Deposition Features and Paleoclimate in Westerly Region of Xinjiang* (Ocean Press, Beijing, ed.1) (in Chinese), pp. 18–62 (2001).
12. Li, C. X., Song, Y. G., Qian, L. B. & Wang, L. M. The history of climate change recorded by the grain size at the Zhaosu loess section in the central Asia since the last glacial period. *Acta Sedimentologica Sinica.* **29**(6), 1170–1179, (2011) (in Chinese with English abstract).
13. Fang, X. M. *et al.* Loess in Kunlun Mountains and its implications on desert development and Tibetan Plateau uplift in west China. *Science in China (Series D. Earth Sciences)* **45**, 289–299 (2002).
14. Porter, S. C., Porter, S. C., Singhvi, A., An, Z. S. & Lai, Z. P. Luminescence age and palaeoenvironmental implications of a late Pleistocene ground wedge on the Northeastern Tibetan Plateau. *Permafrost Periglac.* **12**, 203–210 (2001).
15. Rea, D. K., Leinen, M. & Janecek, T. R. Geologic approach to the long-term history of atmospheric circulation. *Science* **227**, 721–725 (1985).
16. Jin, Z. D., You, C. F., Wang, Y. & Shi, Y. W. Hydrological and solute budgets of Lake Qinghai, the largest lake on the Tibetan Plateau. *Quatern. Int.* **218**, 151–156 (2010).
17. Jin, Z. D. The inorganic carbon budget of Lake Qinghai. *Quatern. Sci.* **30**, 1162–1168 (2010) (in Chinese with English abstract).
18. Colman, S. M., Yu, S. Y., An, Z. S. Shen, J. & Henderson, A. C. G. Late Cenozoic climate changes in China's western interior: a review of research on Lake Qinghai and comparison with other records. *Quatern. Sci. Rev.* **26**, 2281–2300 (2007).
19. Xu, H., Hou, Z. H., Ai, L. & Tan, L. C. Precipitation at Lake Qinghai, NE Qinghai-Tibet Plateau, and its relation to Asian summer monsoons on decadal/interdecadal scales during the past 500 years. *Palaeogeogr. Palaeoclimatol. Palaeoecol.* **254**, 541–549 (2007).
20. Meyers, P. A. & Lallier-vergés, E. Lacustrine sedimentary organic matter records of late Quaternary paleoclimates. *J. Paleolimnol.* **21**, 345–372 (1999).
21. Dykoski, C. A. *et al.* A high-resolution, absolute-dated Holocene and deglacial Asian monsoon record from Dongge Cave, China. *Earth Planet Sci Lett* 233, 71–86(2005).
22. Wang, Y. J. *et al.* Millennial- and orbital-scale changes in the East Asian monsoon over the past 224,000 years. *Nature* **451**, 1090–1093 (2008).
23. Clark, P. U., McCabe, A. M., Mix, A. C. & Weaver, A. J. Rapid rise of sea level 19,000 years ago and its global implications. *Science* **304**, 1141–1144 (2004).
24. Fairbanks, R. G. A 17,000-year glacio-eustatic sea level record: influence of glacial melting rates on the Younger Dryas event and deep-ocean circulation. *Nature* **342**, 637–642 (1989).
25. COHMAP Members. Climatic changes of the last 18,000 years: Observations and model simulations. *Science* **241**, 1043–1052 (1988).
26. Rasmussen, S. O. *et al.* A new Greenland ice core chronology for the last glacial termination. *J. Geophys. Res.* **111**, D06102, doi:10.1029/2005JD006079 (2006).
27. Peterson, L. C., Haug, G. H., Hughen, K. A. & Röhl, U. Rapid changes in the hydrologic cycle of the tropical Atlantic during the last glacial. *Science* **290**(5498), 1947–1951 (2000).
28. Denton, G. H. *et al.* The last glacial termination. *Science* **328**, 1652–1656 (2010).
29. Bond, G. *et al.* Persistent solar influence on north Atlantic climate during the Holocene. *Science* **294**, 2130–2136 (2001).
30. Chen, F. H. *et al.* Holocene moisture evolution in arid central Asia and its out-of-phase relationship with Asian monsoon history. *Quatern. Sci. Rev.* **27**, 351–364 (2008).
31. Liu, X. Q., Shen, J., Wang, S. M., Wang, Y. B. & Liu, W. G. Southwest monsoon changes indicated by oxygen isotope of ostracode shells from sediments in Qinghai Lake since the late glacial. *Chin. Sci. Bull.* **52**, 539–544 (2007).
32. Henderson, A. C. G. & Holmes, J. A. Palaeolimnological evidence for environmental change over the past millennium from Lake Qinghai sediments: A review and future research prospective. *Quatern. Int.* **194**, 134–147 (2009).
33. Li, X. Z., Liu, W. G., Zhang, P. X., An, Z. S. & Zhang, L. Species, valve size, and pretreatment effects on $\delta^{18}O$ and $\delta^{13}C$ values of ostracod valves from Lake Qinghai, Qinghai-Tibet Plateau. *Chem. Geol.* **246**, 124–134 (2007).
34. Denton, G. H. & Broecker, W. S. Wobbly ocean conveyor circulation during the Holocene? *Quatern. Sci. Rev.* **27**, 1939–1950 (2008).
35. Barber, D. C. *et al.* Forcing of the cold event of 8,200 years ago by catastrophic drainage of Laurentide lakes. *Nature* **400**, 344–348 (1999).
36. Murton, J. B., Bateman, M. D., Dallimore, S. R., Teller, J. T. & Yang, Z. Identification of Younger Dryas outburst flood path from Lake Agassiz to the Arctic Ocean. *Nature* **464**, 740–743 (2010).
37. Yu, S. Y. *et al.* Freshwater outburst from Lake Superior as a trigger for the cold event 9300 years ago. *Science* **328**, 1262–1266(2010).
38. Reimer, P. J. *et al.* IntCal04 terrestrial radiocarbon age calibration, 0–26 Cal kyr BP. *Radiocarbon* **46**, 1029–1058 (2004).
39. Steinhilber, F., Beer, J. & Fröhlich, C. Total solar irradiance during the Holocene. *Geophy. Res. Lett.* **36**, L19704, doi:10.1029/2009GL040142 (2009).
40. Denton, G. H. & Karlén, W. Holocene climatic variations-Their pattern and possible cause. *Quatern. Res.* **3**(2), 155–205 (1973).
41. Meehl, G. A., Arblaster, J. M., Matthes, K., Sassi, F. & Loon, H. V. Amplifying the Pacific climate system response to a small 11-year solar cycle forcing. *Science* **325**, 1114 (2009).
42. Damon, P. & Peristykh, A. Radiocarbon calibration and application to geophysics, solar physics, and astrophysics. *Radiocarbon* **42**, 137–150 (2000).
43. Shindell, D. T., Schmidt, G. A., Mann, M. E., Rind, D. & Waple, A. Solar forcing of regional climate change during the Maunder minimum. *Science* **294**, 2149–2152 (2001).
44. Marino, G. *et al.* Early and middle Holocene in the Aegean Sea: interplay between high and low latitude climate variability. *Quatern. Sci. Rev.* **28**, 3246–3262 (2009).
45. Henderson, A. C. G., Holmes, J. A. & Leng, M. J. Late Holocene isotope hydrology of Lake Qinghai, NE Tibetan Plateau: effective moisture variability and atmospheric circulation changes. *Quatern. Sci. Rev.* **29**, 2215–2223 (2010).
46. Zhou, W. J. *et al.* High-resolution evidence from southern China of an early Holocene optimum and a mid-Holocene dry event during the past 18,000 years. *Quatern. Res.* **62**, 39–48 (2004).
47. Slota, P. J. J., Jull, A. J. T., Linick, T. W. & Toolin, L. J. Preparation of small samples for ^{14}C accelerator targets by catalytic reduction of CO. *Radiocarbon* **29**, 303–306 (1987).
48. Jull, A. J. T. in *Encyclopedia of Quaternary Science,* eds Elias S. A. (Elsevier, Amsterdam), pp. 2911–2918 (2007).
49. Weninger, B., Jöris, O. & Danzeglocke, U. CalPal-2007, Cologne Radiocarbon Calibration & Palaeoclimate Research Package. http://download.calpal.de/calpal-download/
50. Zhou, W. J. *et al.* The mean value concept in mono-linear regression of multi-variables and its application to trace studies in geosciences. *Science in China (Series D. Earth Sciences)* **50**, 1828–1834 (2007).
51. Lu, H. Y. & An, Z. S. Pretreated methods on loess-palaeosol samples granulometry. *Chin. Sci. Bull.* **43**, 237–240 (1998).
52. Li, X. Z., Liu, W. G., Zhang, L. & Sun, Z. C. Distribution of recent ostracod species in the Lake Qinghai area in northwestern China and its ecological significance. *Ecol. Indic.* **10**, 880–890 (2010).
53. Liu, W. G., Li, X. Z., Zhang, L., An, Z. S. & Xu, L. M. Evaluation of oxygen isotopes in carbonate as an indicator of lake evolution in arid areas: The modern Qinghai Lake, Qinghai-Tibet Plateau. *Chem. Geol.* **268**, 126–136 (2009).
54. Kalnay, E. *et al.* The NCEP/NCAR 40-year reanalysis project. *Bull. Am. Meteorol. Soc.* **77**, 437–471 (1996).
55. Berger, A. M. & Loutre, F. Insolation values for the climate of the last 10 million years. *Quatern. Sci. Rev.* **10**, 297–317 (1991).

Acknowledgment

We thank Professors Guoxiong Wu, John Kutzbach, Gorge Denton and Steve Clemens for discussion and valuable suggestions and Professors Sumin Wang, Stephen C. Porter, Ji Shen, Liping Zhou, Peizhen Zhang, Jule Xiao and Li Li for kind help in this study. This work was jointly funded by the International Continental Drilling Program, the National Natural Science Foundation of China, the Ministry of Science and Technology of China, Chinese Academy of Sciences and the U.S. National Science Foundation.

Author contribution

An Zhisheng: overall coordination of writing, drilling, sedimentology, ^{14}C dating and palaeoclimatic interpretations; Steven M. Colman: writing, drilling, sedimentology and palaeoclimatic interpretations; Weijian Zhou, A. J. Timothy Jull, Xuefeng Lu and Peng Cheng: ^{14}C dating and age-model construction; Eric T. Brown: sedimentology and palaeoclimatic interpretations; Xiaoqiang Li, Hong Chang, Yougui Song, Xiaoke Qiang, and Li Ai: drilling, sampling and core description; Yanjun Cai: writing, speleothem record and palaeoclimatic interpretations; Xiaodong Liu, Libin Yan and Zhengguo Shi: regional climate context and palaeoclimatic interpretations; Youbin Sun and Jibao Dong: separation of eolian dust and riverine components and establishment of Westerlies climate index; Weiguo Liu and Xiangzhong Li: ostracod analyses; Hai Xu: TOC analyses. All other 8 authors contributed to core description, acquisition, analysis and interpretation of data presented in this paper. All authors reviewed the manuscript.

Additional information

Supplementary information accompanies this paper at http://www.nature.com/scientificreports

Competing financial interests: The authors declare no competing financial interests.

How to cite this article: An, Z. *et al*. Interplay between the Westerlies and Asian monsoon recorded in Lake Qinghai sediments since 32 ka. *Sci. Rep.* **2**, 619; DOI:10.1038/srep00619 (2012).